Droplet spreading in a chiral active fluid

Jessica Metzger, William Irvine

May 12, 2022

1 Introduction

We are all familiar with the behavior of ordinary fluids like water and honey. Zooming in on any such fluid, the particles interact through attractive and repulsive forces, which are parallel to the line between them, producing intuitive notions of viscosity (resistance to shear) and surface tension (minimization of surface area). However, we can also consider fluids where forces between particles are perpendicular to the line between them. Such interactions break time-reversal and parity symmetry, and are described by non-equilibrium statistical mechanics, requiring external forcing. Examples are colonies of spinning bacteria, chiral vortex fluids, and quantum hall fluids (where time-reversal symmetry is broken by the external magnetic field). Hydrodynamic descriptions of these fluids often require additional linear response coefficients, such as an odd viscosity that breaks Onsager reciprocity [1].

Recent experiments in the Irvine lab create chiral forces by spinning magnetic particles with an external magnetic field [2, 3]. This two-dimensional colloidal fluid is submerged in water and resting on a glass slide, and the spinning of each colloidal particle generates a vortex that interacts tangentially with other vortices, inducing patterns of frustration describable by a hydrodynamic theory with odd viscosity. A schematic of the interaction between colloidal particles and of the experimental setup is shown in Fig. 1.

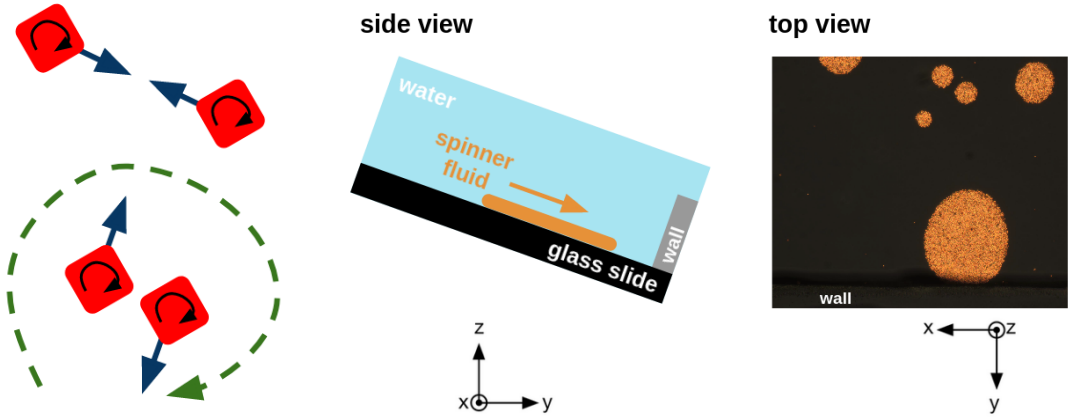

Figure 1: *Left: a schematic of the interactions between two colloidal particles spinning clockwise. The vortex pair interaction induces clockwise rotation of the pair. Middle: a schematic of the setup of our experimental system. Right: an image from the experiment.*

These fluids were introduced and studied with experiments, simulation, and theory in [2, 3], with estimations of the hydrodynamic parameters. The hydrodynamic theory was tested mainly by studying the behavior of the fluid's boundary. It is observed that the fluid is made up of co-rotating patches of local hexagonal order, which are larger when the spinner frequency is lowered. A prominent edge current with the same chirality as the spinners is also observed. We seek to better understand these 2D active chiral fluids, including confirming the estimates of system parameters, and modeling the behavior of the fluid in classic situations such as droplet spreading and thin film wetting.

In this thesis, we examine droplet spreading in chiral fluids. Starting with experiments and simulations of droplets spreading under the influence of gravity, we derive a theory of droplet spreading within the framework of chiral hydrodynamics and seek to compare this theory with experiments. In section 2, we describe classical droplet spreading theory in even fluids with dimensional analysis and elementary arguments, comparing estimates to simulation and experiment and revealing the pitfalls of neglecting the chirality. In section 3, we describe classical thin film theory and adapt it to our chiral fluids, uncovering a regime where the hydrodynamic theory is inapplicable.

2 Classical droplet spreading

Our experiment consists of 2D droplets sedimented on a wall, as depicted in Fig. 1. Droplet spreading in ordinary fluids is a well-studied classical problem. The initial evolution is described by power-law expansion, with the exponent determined by the balance between dominant dissipating and driving forces [4, 5]. We start out by investigating the spreading of achiral 2D droplets, and seeing how much of the spreading behavior of our droplets can be explained by this theory.

Our fluid has even viscosity η and surface tension γ. The motion has velocity v and is overdamped, with a substrate drag force per unit area Γv caused by motion against the glass plate. The fluid is effectively incompressible, with density ρ and volume V, and as depicted in the schematic (Fig. 1), our glass plate is tilted by an angle θ so that the fluid sediments against a wall, experiencing a gravitational force per unit area of $\rho g \sin\theta$ which we often abbreviate to ρg. At any given moment, the droplet has radius r (half the diameter).

2.1 Dimensional Analysis

Use dimensional analysis on these parameters to deduce the form of the radial expansion equation of motion. The 8 relevant variables $\rho, V, g, \Gamma, \eta, \gamma, r, \dot{r}$ of 3 dimensions give 5 independent dimensionless variables by Buckingham's Π theorem, but in the absence of knowledge of which are most relevant, we include three extra, as in [5]:

$$\frac{\Gamma\dot{r}V/r}{\gamma/r}, \quad \frac{\Gamma\dot{r}V/r}{\rho g V/r}, \quad \frac{\eta r\dot{r}/V}{\gamma/r}, \quad \frac{\eta r\dot{r}/V}{\rho g V/r}, \quad \frac{V}{r^2}, \quad \frac{\rho r\dot{r}}{\eta}, \quad \frac{\rho r\dot{r}}{\Gamma V} \tag{1}$$

The first 4 are ratios between possible dissipation and driving mechanisms (with numerator and denominator each representing a characteristic force per unit length of these mechanisms), V/r^2 is a geometric scale, and the last two are Reynold's numbers.

If the Reynold's numbers are small (which is true for our overdamped system), and if one driving and one dissipation mechanism dominates (as is often the case [4]), dimensional analysis tells us the evolution of the radius should be governed by

$$\Pi = \frac{\dot{r}}{v} = f(V/r^2) \tag{2}$$

where Π is the dimensionless variable representing the ratio between the dominant driving and dissipation mechanisms, which is always of the form $\dot{r}/v$ for some characteristic velocity v.

2.2 Equation of motion

Look into physics to determine the exact form of eq. 2. The droplet expansion can be driven by gravity and surface tension (in the "hydrophilic" case where surface wetting is energetically favorable). Energy can be dissipated through viscosity, substrate drag, and surface tension (in the "hydrophobic" case). Given the estimates of the hydrodynamic parameters in [2], the driving should be dominated by gravity and the dissipation should be dominated by substrate drag. The overall evolution can be found by equating the dissipated power P_Γ and driving power P_g, which gives

$$\frac{\dot{r}\Gamma}{\rho g} = \frac{3}{4}\frac{V}{r^2} \tag{3}$$

which matches our predictions from dimensional analysis, eq. 2. Here, the characteristic velocity is the sedimentation velocity, $v_{sed} = \rho g/\Gamma$, which can be easily measured in experiments. It has the solution

$$r(t) = \left(\alpha\frac{\rho g V}{\Gamma}(t - t_0) + r_0^3\right)^{1/3}. \tag{4}$$

where $\alpha = 9/4$. If the spread is a Poiseuille flow without slipping, on the other hand, we will have $\alpha = 5/6$. In both cases, the exponent of the power-law is $1/3$.

2.3 Comparison to simulation

Yehuda Ganan in the Irvine lab performed simulations of droplets of the chiral active fluid spreading. Details of these simulations can be found in [3]. The gravity experienced by particles was varied, along with the total droplet volume and the particle spinning frequency.

Does the simulated data match our classical predictions? There is no boundary physics programmed into the wall, so we assume a slipping flow, and test eq. 4 against the simulated data. We know the relevant parameters of the simulated system (gravity and substrate drag), so there are no free parameters in this test. The data and predictions are plotted in Fig. 2.

Initial inspection of the radius over time gives an approximate $r \propto t^{1/3}$ evolution, as expected for the model. With no fitting parameters, the theory gives good predictions for the behavior in the observed regimes, as can be seen in Fig. 2. At lower frequencies, the agreement is worse, which may be due to the better lattice order of the droplet. We expect the spread at lower frequencies to be closer to a viscoelastic deformation, which may require going beyond the hydrodynamic model.

Overall, it seems the radial evolution of our simulated odd droplets matches a gravitationally-driven, drag-dampened spread for a classical even droplet.

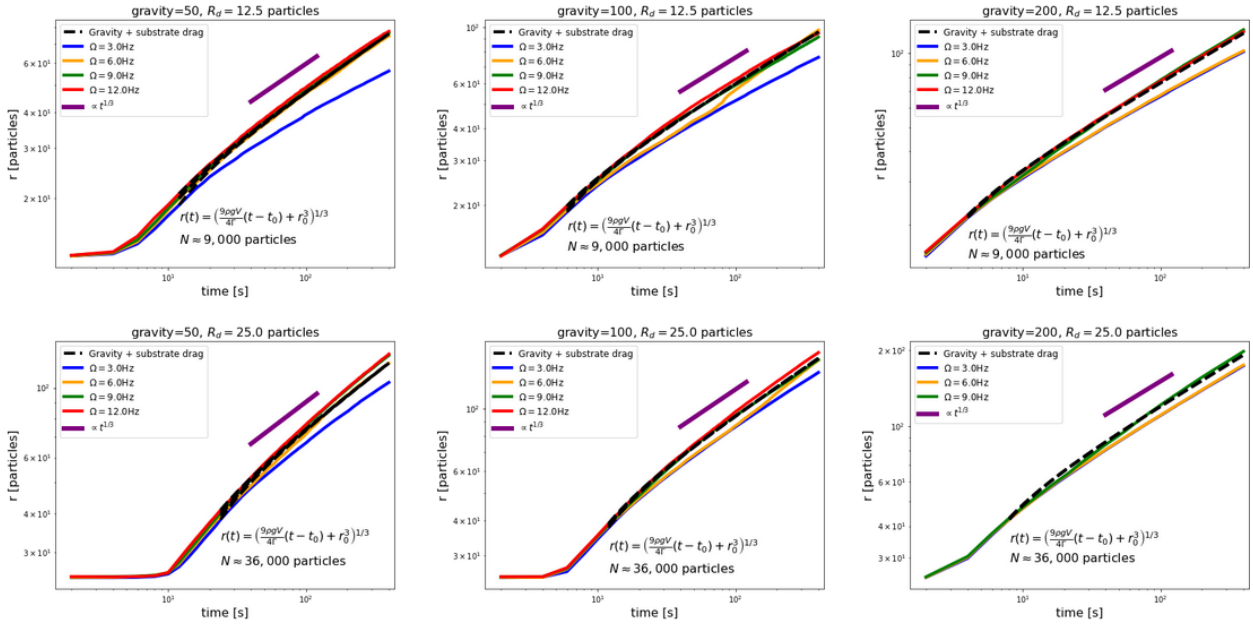

Figure 2: *Simulated chiral droplet radius over time (colors), with the model predictions for spread dominated by gravity vs. substrate drag (black). There are no fit parameters.*

2.4 Comparison to experiment

Ephraim Bililign in the Irvine lab performed experiments on droplets of the fluid, depositing them on a wall. The details of these experiments can be found in [2, 3]. From these videos, we extract the droplet radius over time. First, we compare our predictions to the non-chiral version of our fluid, then test it out on the chiral version.

2.4.1 Non-chiral droplets

The non-chiral analogue of our experimental fluid can be created by alternating the rotation direction of the magnetic field every 10-50 cycles. We expect such a fluid to have the same even viscosity η and surface tension γ, but to lack the characteristic edge current. We look at the spreading behavior of two non-chiral droplets and compare it to our predictions. A few frames from the evolution of each droplet are shown in Fig. 3.

Because the colloidal particles experience friction with the wall, we expect the flow to be a non-slipping shear, governed by eq. 4. Because we can measure the droplet sedimentation velocity, there are no free parameters in this test of the theory. Comparison between the observed non-chiral droplet radial expansion and the predicted expansion determined by gravity and substrate drag is shown in Fig. 4. The agreement with theory is relatively good, given the available data.

2.4.2 Chiral droplets

Next, we test our theory on the chiral experimental droplets. In addition to the classical viscosity η, surface tension γ, gravity, and substrate drag Γ, there is an odd viscosity η_o and rotational viscosity η_R induced by the constant particle spinning at frequency Ω [2]. Moreover, there is an edge current

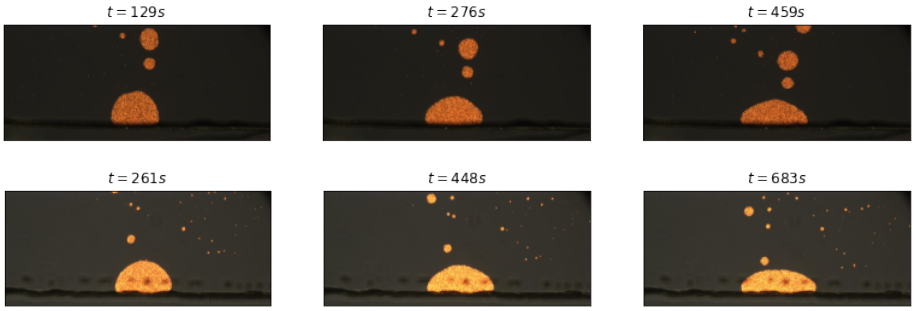

Figure 3: *The spreading behavior of two non-chiral droplets. The magnetic field spins at 10Hz in alternating directions to remove the chirality. The above and below droplets correspond to the left and right plots of Fig. 4, respectively.*

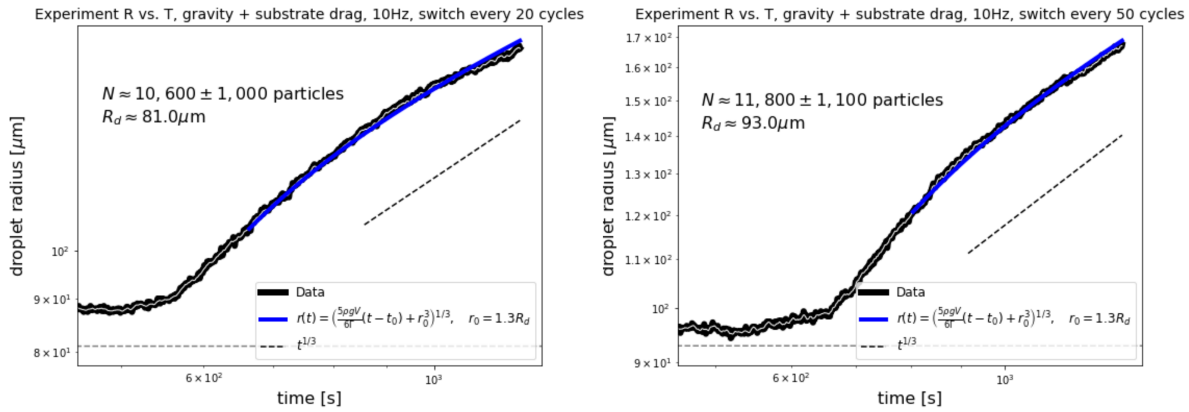

Figure 4: *Radial evolution of two experimental non-chiral droplets, along with the theoretical predictions for no-slip spread dominated by gravity vs. substrate drag. The magnetic field spins at 10Hz, and spin direction is switched every 20 or 50 cycles, respectively, to remove the chirality. The left plot corresponds to the above droplet in Fig. 3, and the right plot corresponds to the below droplet in Fig. 3. There are no fit parameters.*

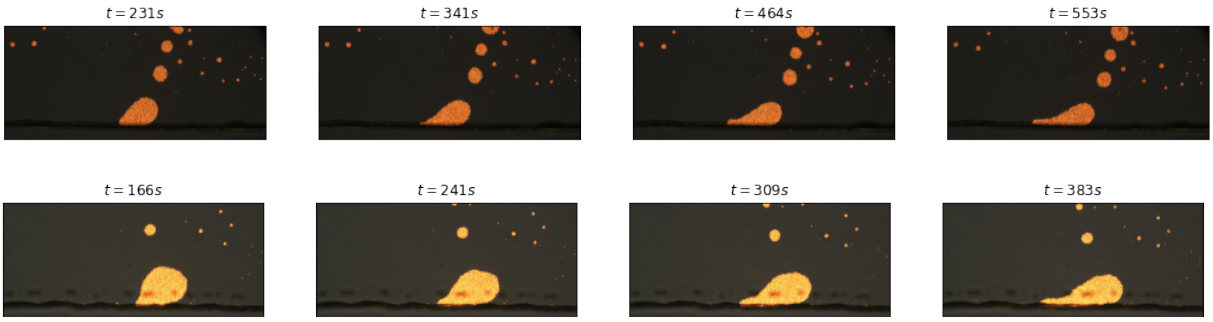

Figure 5: *The evolution of two chiral droplets at various stages, with spin frequencies* Ω *=10Hz (above) and 5Hz (below). Spin is counter-clockwise. One can see the thin film being extruded from the main droplet in one preferred direction.*

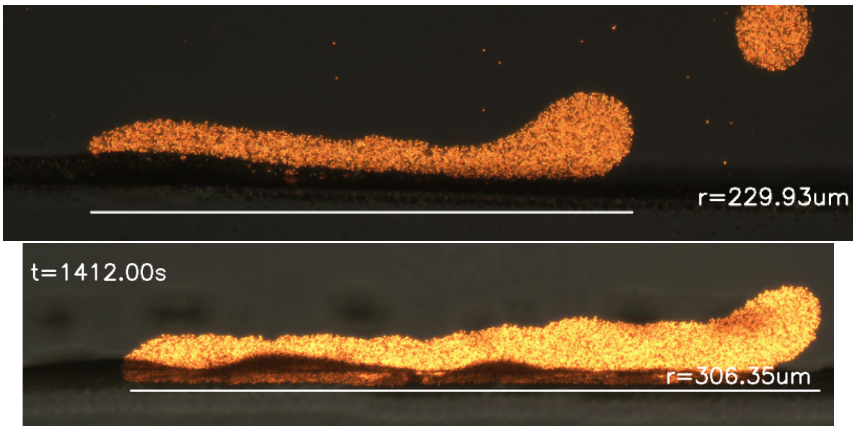

Figure 6: *Long-time behavior of a spreading chiral droplet at spinning frequency* Ω *=10Hz (above) and 5Hz (below). The spreading behavior can't be described by classical droplet spreading theory.*

along the droplet boundary with Ω's chirality, so there is friction against the wall in a preferred direction. A thin film is extruded from the droplet in one direction because of this friction. The flow is no longer a simple shearing spread where gravitational driving balances drag dissipation.

The early evolution of two chiral droplets is shown in Fig. 5, where this pulling effect is evident. Indeed, videos of the long-term behavior of the chiral droplets show a dramatic extrusion of the droplets into a thin film (Fig. 6). When comparing the classical radial expansion model to this spreading behavior, the predicted spread is much too slow. It fails to account for the additional driving provided by this base stress.

3 Crawling films

We have lost the left-right symmetry needed to apply classical droplet spreading theory. However, we can now use the flat film symmetry of these crawling droplets to develop different theory. We use the hydrodynamic descriptions of these fluids (described in supplementary section 6 of [2]) to predict the behavior of these flat films in various situations, and compare those predictions to

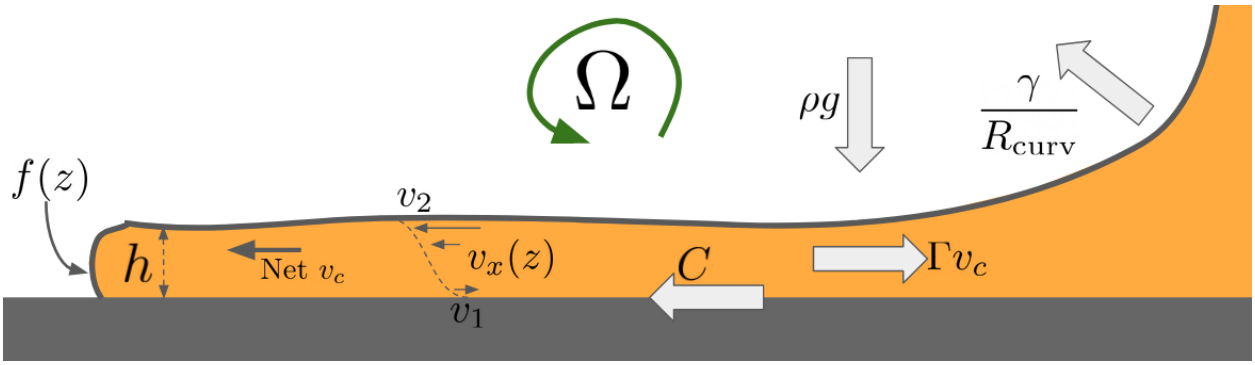

Figure 7: *Our model for the crawling thin film.*

experiment. A model summarizing the theory behind these predictions is shown in Fig. 7.

3.1 Flat film

We first develop the theory for a flat film geometry. Each film is relatively flat, with a constant height and a constant crawling velocity (see e.g. Fig. 6 for a snapshot of a film). In a free-floating finite slab of the fluid with height h, there is a velocity field

$$\boldsymbol{v}(\boldsymbol{x}) = \hat{\boldsymbol{x}} \left(\frac{2\Omega\delta\eta_R}{\eta + \eta_R} \right) \frac{e^{-z/\delta} - e^{z/\delta}}{e^{h/2\delta} - e^{-h/2\delta}}. \tag{5}$$

This is calculated in supplementary section 6.3.2 of [2]. This demonstrates the edge current with penetration depth δ flowing in the $-\Omega$ direction at the top edge of the slab, and in the Ω direction on the bottom edge.

A slab sitting against a wall experiences friction from the motion of the edge current against the wall. This frictional stress, C, causes the vorticity at the bottom edge to be dampened, slowing the Ω-direction base edge current while leaving the top surface's edge current unchanged (supposing that the system is overdamped, so that no information travels from the base to the top). This "treadmilling" effect causes net transport of fluid in the $-\Omega$ direction, resulting in the observed crawl.

Let's solve the equations of motion for this geometry to see if there are physical predictions for the height and crawl velocity. The equations of motion are [2]

$$\begin{aligned} \nabla \cdot \boldsymbol{\sigma} - \Gamma \boldsymbol{v} - \rho \boldsymbol{g} = \partial_j \sigma_{ij} - \Gamma v_i - \rho g_i = 0 \\ \nabla \cdot \boldsymbol{v} = \partial_j v_j = 0 \end{aligned} \tag{6}$$

The top equation is the momentum equation, where the internal stresses σ_{ij} give rise to forces $\partial_j \sigma_{ij}$ which are balanced against gravity $-\rho g_i$ and drag $-\Gamma v_i$. The second equation is the incompressibility condition. The stress σ_{ij} is given by

$$\sigma_{ij} = -\delta_{ij}(p + \eta_o \omega) + \eta_R \epsilon_{ij}(2\Omega - \omega) + \eta(\partial_i v_j + \partial_j v_i) + \eta_o(\partial_i \epsilon_{jk} v_k + \partial_j \epsilon_{ik} v_k) \tag{7}$$

which includes pressure, ordinary viscous stresses from η, odd viscous stresses from η_o, and the vorticity-inducing stresses of rotational viscosity η_R. The stress boundary condition is

$$\sigma_{ij} n_j = \begin{cases} n_i \gamma \kappa, & z > 0 \\ n_i \gamma \kappa - t_i C, & z = 0 \end{cases} \tag{8}$$

which includes the surface tension $\gamma\kappa$ and the tangential stress from resistance to motion at the base C. For our flat slab geometry, after some computation, these equations are solved by a velocity profile of the form

$$\boldsymbol{v}(\boldsymbol{x}) = \hat{\boldsymbol{x}} \frac{\delta e^{-h/2\delta}}{\eta + \eta_R} \left[(2\Omega\eta_R - C)\, e^{-z/\delta} - 2\Omega\eta_R e^{z/\delta} \right]. \tag{9}$$

The base stress C merely adds a perturbation to eq. 5, as expected.

3.1.1 Thin film equation

Suppose now that we allow slight fluctuations in the height. One can often simplify the equation of motion of a fluid which is relatively thin and flat in one dimension to a PDE where the change in height is expressed as the divergence of some height flux, a "thin film equation" [6]. For our fluid, the governing thin film equation is

$$\partial_t h = -\partial_x \left[\frac{h}{\Gamma} \partial_x (\gamma \partial_x^2 h - g h) \right]. \tag{10}$$

This is similar to the thin film equation describing the thickness of a thin bridge between two masses of fluid in a Hele-Shaw cell [7].

3.1.2 Physical predictions

We now examine the physical predictions generated by this theory. First, we examine the height and crawling velocity. Let $v_1 = v(-h/2)$ be the base velocity, and $v_2 = v(h/2)$ be the top surface velocity. Assume $\delta \ll h$, which is reasonable given that $\delta \approx 4.5\mu$m for a fluid with film height $h \approx 45\mu$m, and an estimate for deviations from this assumption for $h = 2\delta$ is approximately 2% for all quantities. The net crawl velocity can be readily estimated by the sum of the mass fluxes of the edge currents divided by the height. We find a crawl velocity

$$v_c = \frac{\delta}{h}(v_1 + v_2) \approx -\frac{C}{\Gamma h}. \tag{11}$$

Immediately, we see that the theory gives no prediction for v_c or for h, only for the relationship between them. We do get an estimate for the net crawling flux, $j = v_c h = -C/\Gamma$. The net crawl, arising from the difference in mass flux in the upper and lower edge currents, is determined by the stress C at the base.

Qualitatively, something is off: the thinner film (Fig. 6, top) crawls more slowly than the thicker film (Fig. 6, bottom); thus the thin film must have a significantly lower flux j. However, it makes much more sense from the hydrodynamic perspective that a film with a faster spinning frequency of $\Omega = 10$Hz should crawl faster, for example, if C depends on edge velocity (which is proportional to Ω).

We can also check the predicted edge velocities and see if they are physically feasible. We observe crawling velocities of about $v_c \approx -0.7\mu$m/s and heights of $h \approx 45\mu$m when $\Omega = 5$Hz.

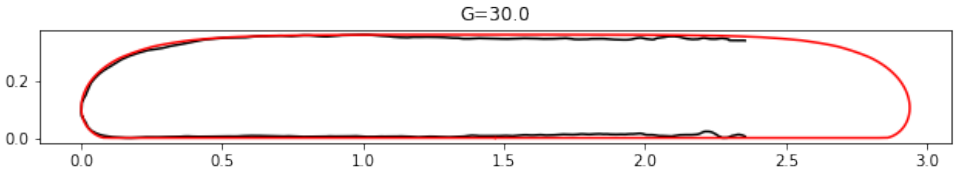

Figure 8: *Comparison of the real equilibrium chiral droplet tip (black) with the equilibrium droplet profiles computed by surface evolver (red).*

Given the known substrate drag $\Gamma = 2.4 \times 10^{-9} \mu\text{P}\cdot\text{s}/\mu\text{m}$, so this suggests a base stress of about $C \approx 7.6 \times 10^{-8}$ kg/s^2.

Now consider the required base edge velocity $v_1 = v(-h/2)$ to explain this mass flux. We find

$$v_1 = \frac{2\Omega\eta_R\delta - C\delta}{\eta + \eta_R} \approx -6\mu\text{m/s}. \tag{12}$$

The base edge current, which should be positive (and merely dampened by the base friction), is severely negative. It turns out, there is no model for the base friction that accounts for a crawl velocity as high as the observed -0.7μm/s. We must look beyond the hydrodynamic model to explain this behavior.

3.2 Film tip

Before discarding the hydrodynamic theory, let's examine other regions beyond the flat film and see if the hydrodynamic theory explains their geometry and evolution. First, consider the film tip.

Consider the tip of the droplet and the curve it defines in space ($f(z)$ in Fig. 7). It is relatively constant over time, as the droplet crawls but doesn't change shape. This is reminiscent of the curve defined by an ordinary zero-wetting droplet that has spread under gravity. We begin by looking at steady-state droplet profiles for 2D zero-wetting droplets spreading under gravity using surface evolver. This profile is shown as the red curve in Fig. 8.

We then extract the steady-state geometry from the experimental images of the 5Hz droplet (Fig. 6, below). We averaged it out by lining up the leftmost x-coordinate, sorting the top and bottom halves from left to right, and averaging them. This gives us a curve in space, which we can use as a fixed geometry for our system. We find that this curve does indeed match the high-gravity (flat pancake limit) equilibrium achiral droplet profiles computed by surface evolver. This correspondence is shown in Fig. 8.

So maybe the droplet geometry can be described as an achiral droplet with a different effective surface tension. No such description is immediately evident. We need to use a numerical approach, solving the equations of motion on this domain and finding a velocity profile that maintains the geometry. This approach, with preliminary results, is described below.

3.3 Numerics

A good way to test the hydrodynamic theory is to solve it on the observed domain and check for stability and matched behavior (e.g. stable crawling of a thin film with the same geometry and velocity). We solve the equations of motion (eq. 6, 7) on domains where the flows are either observable or analytically solvable. We work in FEniCS, for which we must convert the equations

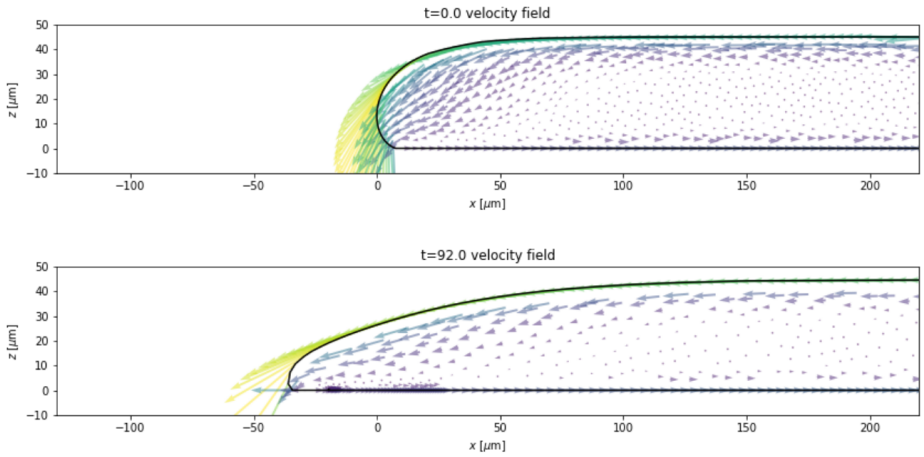

Figure 9: *The velocity field for the crawling film tip, computed using FEniCS, and evolved for almost 100s with a timestep of dt=0.01s.*

of motion to their weak form, also including the boundary stresses as Von Neumann or Dirichlet boundary conditions. We use the parameter estimates (η, η_o, Γ, etc.) from [2].

First, we compute the velocity field $\boldsymbol{v}$ for flat floating slab (eq. 5). We find exact agreement between the numerical solution and the theoretical predictions. Next, we test the solution on a domain shaped like the crawling droplet tip (Fig. 8). We incorporate surface tension and friction at the base via the stress boundary conditions (eq. 8). We include a Dirichlet boundary condition for the velocity profile at the right edge based on the theoretical prediction for a sitting slab (eq. 9); far from the boundary, this condition has no effect and the velocity profile assumes this form anyways. We then evolve the domain by incrementing each boundary point by $\boldsymbol{v}dt$ for a fixed dt. The resulting velocity profile, and the evolved profile after $\sim$100s, are shown in Fig. 9.

Not only is a crawling velocity as high as -0.7μm/s theoretically unexplainable (as explained in sec. 3.1.2), but we find that the geometry of the film tip is unstable under time evolution regardless of the crawl speed (Fig. 9). This is true for any model of base friction. This confirms the prediction that we need to move beyond the hydrodynamic model to explain the crawling of these thin films.

4 Conclusions

The 2D active chiral colloidal fluids studied in the Irvine Lab seem to be described by a hydrodynamic theory with extra "odd" terms [2, 3]. However, tests of this theory have been limited largely to perturbations of the fluid boundaries. In order to test the theory on bulk deformations, we develop theory for droplet spreading in these fluids. Predictions are accurate for simulated chiral droplets and for experimental achiral droplets, suggesting the applicability of the hydrodynamic theory in these regimes. However, in experimental chiral droplets, friction from the edge current prevents us from applying classical droplet spreading theory to the resulting crawling flat films. After developing the theory for these films, we find that the hydrodynamic theory is unable to explain the fast crawl and the steady-state geometry of the experimental chiral films. We are continuing to work on developing theory to explain this behavior.

5 Acknowledgements

Experiments were performed by Ephraim Bililign. Simulations were performed by Yehuda Ganan. The author would like to thank her advisor and other members of the lab for lots of helpful guidance.

References

[1] J. E. Avron. Odd Viscosity. *Journal of Statistical Physics*, 92:543–557, May 1998.

[2] Bililign E.S. Magkiriadou S. et al. Soni, V. The odd free surface flows of a colloidal chiral fluid. *Nature Physics*, page 1188–1194, 06 2019.

[3] Ephraim Bililign, Florencio Balboa Usabiaga, Yehuda Ganan, Vishal Soni, Sofia Magkiriadou, Michael Shelley, Denis Bartolo, and William Irvine. Chiral crystals self-knead into whorls. 02 2021.

[4] Daniel Bonn, Jens Eggers, Joseph Indekeu, Jacques Meunier, and Etienne Rolley. Wetting and spreading. *Rev. Mod. Phys.*, 81:739–805, May 2009.

[5] Sylvia Durian, Sam Dillavou, Kwame Markin, Adrian Portales, Bryan Maldonado, William Irvine, Paulo Arratia, and Douglas Durian. Spatters and spills: Spreading dynamics for partially wetting droplets. 11 2021.

[6] Alex Oron, Stephen Davis, and S. Bankoff. Long-Scale Evolution of Thin Liquid Films. *Reviews of Modern Physics*, 69:931–980, July 1997.

[7] Peter Constantin, Todd F. Dupont, Raymond E. Goldstein, Leo P. Kadanoff, Michael J. Shelley, and Su-Min Zhou. Droplet breakup in a model of the hele-shaw cell. *Phys. Rev. E*, 47:4169–4181, Jun 1993.